Ab initio study of electron affinity variation induced by organic molecule adsorption on the silicon (001) surface

Ivo Borriello,[1,*] Giovanni Cantele,[1] Domenico Ninno,[1] Giuseppe Iadonisi,[1] Maurizio Cossi,[2] and Vincenzo Barone[2]
[1]*Coherentia CNR-INFM and Dipartimento di Scienze Fisiche, Università di Napoli "Federico II," Complesso Universitario Monte Sant'Angelo, Via Cintia, I-80126 Napoli, Italy*
[2]*INSTM and Dipartimento di Chimica, Università di Napoli "Federico II," Complesso Universitario Monte Sant'Angelo, Via Cintia, I-80126 Napoli, Italy*

(Received 26 March 2007; revised manuscript received 11 June 2007; published 24 July 2007)

The effect of organic adsorbates on the silicon (001) surface is investigated using first-principles calculations. Ethylene and a class of cyclopentene derivatives, containing different functional groups, are considered, all anchoring to the surface through the same [2+2] cycloaddition mechanism. Because they all show similar bonding properties, any variation in the surface properties must be related to the functional group. The structural relaxation induced by the adsorption is discussed, elucidating the effect of both the adsorbate species and coverage. It turns out that different distortions occur in the molecular geometry, depending on both the species and the surface coverage, while molecule-to-surface bonding does show very similar features for all the considered molecules. We show that the presence of the adsorbate can modify the surface charge density, thus giving rise to an induced dipolar layer that modifies the electrostatic potential outside the surface. Such a dipole layer can, in turn, be related to surface electron affinity and work function changes. A careful analysis of the dipole moment and of the electrostatic potential changes is carried out discussing the correlations with the properties of the isolated molecules. All the results indicate how the surface properties can be tuned through a suitable choice of the adsorbate.

DOI: 10.1103/PhysRevB.76.035430 PACS number(s): 68.43.Bc, 68.47.Fg, 73.20.−r, 85.65.+h

I. INTRODUCTION

Hybrid organic-inorganic compounds are expected to play a crucial role in future technologies and devices. The matching of the best properties of the organic and inorganic phases gives a unique opportunity of obtaining new systems with tunable optical, electric, and mechanical properties.[1–7] A wide range of applications (sensing and biosensing, optoelectronics, drug delivery, etc.) is expected to come in the near future, and many routes are being pursued toward new generations of functional materials.[1,6] Among them, we cite surface functionalization that consists in transforming surfaces in interfaces.[3,7–9] Huge efforts have been spent toward the controlled modification (at atomic level) of surfaces where a proper choice of both the substrate and the covering layer is needed.

Silicon (Si) surfaces have been the subject of intensive investigations.[2,4,5,10] The possibility of integration of current Si-based microelectronics within new functional devices is believed to be a breakthrough of the future. The silicon (001) surface is particularly suitable to functionalization with organic molecules containing a double C=C bond.[2–5,11] This is due to the particular surface reconstruction whose main feature is the formation of asymmetric (tilted) Si dimers.[5,10] Indeed, the bonding nature of a Si dimer, though still debated, can at least formally be described in terms of a double Si—Si bond (in analogy with the double C=C bond found in alkenes). Nonetheless, at variance with the double C=C bond, the charge density associated with the π component of the bond is thought to be asymmetrically distributed over the two atoms. This results in tilted Si—Si dimers,[5] in which the "second" (π) bond is much weaker than in organic molecules. The consequences of that are rather significant: the adsorption of organic molecules containing a double C=C bond can occur through a mechanism known as a [2+2] cycloaddition in organic chemistry.[2,4,12] The π bond in both the surface dimer and the organic molecule breaks, with the formation of two C—Si σ bonds. This reaction is known to occur even at room temperature, with relatively small activation barriers. The dimer buckling does play a relevant role in the adsorption process, as the same reaction is forbidden (with a huge activation barrier) between two double bonded C=C groups.

In this paper, first-principles calculations of adsorbed organic layers on the silicon (001) surface are presented. In particular, we focus on the changes in the surface electron affinity induced by the coverage by considering ethylene (C_2H_4) and a class of cyclopentene derivatives C_5H_6-R_1R_2 containing different functional groups. The adsorption induces the formation of a surface dipole layer that, in turn, can enhance or reduce the ability of extracting electrons from the surface. The structural and electronic properties of the different adsorbate-covered surfaces are analyzed in some detail with an emphasis on the different contributions setting up the dipolar layer. Moreover, we have made an attempt to correlate the molecular dipole moments before and after the adsorption on the Si surface.

The paper is organized as follows. In Sec. II A, the technical details on the performed calculations are summarized. The main concepts concerning electron energetics at the semiconductor surface and semiconductor-adsorbate interface are outlined in Secs. II B and II C. These concepts are applied to the specific case of the adsorption of ethylene and a class of cyclopentene derivatives on the silicon (001) surface in Sec. III. Finally, in Sec. IV, some conclusions are drawn.

II. THEORETICAL METHOD

A. General

The calculations have been performed using a plane-wave, pseudopotential method based on the density functional theory (DFT), as implemented in the Quantum ESPRESSO package.[13] The Si atoms have been represented using a norm conserving pseudopotential built within the Rabe-Rappe-Kaxiras-Joannopoulos (RRKJ) scheme.[14] In the case of C, N, and H, we have selected ultrasoft pseudopotentials constructed within the same RRKJ scheme. The Perdew-Burke-Ernzerhof approximation for the exchange-correlation functional has been adopted.[15] The electronic wave functions have been expanded using plane waves corresponding to energies up to 30 Ry, while a 180 Ry cutoff energy has been used to represent the total charge density.

The $p(2\times2)$ reconstructed clean silicon (001) surface is modeled as an extended slab using a supercell containing 12 layers of silicon (Si), with four Si atoms per layer, and a vacuum region as thick as 14 Si atomic layers (19 Å). The surface in-plane crystal cell (assumed to be in the xy plane) was built using the optimized bulk Si lattice constant of 5.47 Å, to be compared with the experimental result[16] of 5.43 Å. Full relaxation of all the atoms but those belonging to the two central Si layers was allowed. The optimized geometries are obtained using the Hellman-Feynman forces with the Broyden-Fletcher-Goldfarb-Shanno algorithm to minimize the total energy with respect to the atomic positions. The surface Brillouin zone was sampled using a $(2\times2\times1)$ Monkhorst-Pack k-point grid.[17]

The adsorbed molecules were placed on both sides of the slab to ensure inversion symmetry, so minimizing the formation of artificial electric fields in the vacuum.[18] The same supercell as that used for the clean surface has also been used in all the calculations (with a minimum vacuum region thickness equivalent to six silicon atomic layers). No significant variations of the calculated properties were found on increasing the vacuum region.

The surface dipole moments induced by the molecules are investigated with a detailed analysis of both the charge density distribution and the electrostatic potential. Because we deal with a surface problem, planar averages on planes parallel to the surface are carried out for the main quantities of interest (see Sec. II C). For the evaluation of the variations of the electron affinity and ionization potential induced by surface adsorbates, the knowledge of the vacuum level is needed. The latter can be easily determined from the value of the averaged electrostatic potential far enough from the surface. However, the systematic comparison of the vacuum level in the presence of different adsorbates needs an alignment procedure bringing the zero of the energy to the same value for all the considered systems. The one-dimensional planar average of the electrostatic potential shows microscopic oscillations that, in our case, almost perfectly reproduce a bulklike behavior in the middle of the slab, as it will be shown in Sec. III B 3 (the bulk potential was computed using the same surface supercell and the same number of Si atoms, after removing the vacuum region). To get rid of such oscillations, this potential can be further averaged on a "macroscopic" window, and the value of the new average at the center of the slab can be used for the alignment procedure (so as to match the bulk value). Therefore, the difference between the value of the macroscopically averaged potential at the center of the slab of a given (clean or covered) surface and that in bulk Si is computed. Finally, both the potential and the band structure of the given surface are shifted by this difference. It is worth pointing out that for the alignment procedure to be meaningful, it is necessary that the center of the slab reproduces a common environment in all the cases. In the rest of the paper, the shown potentials and band structures are meant to have been shifted according to what is explained above.

The optimized geometry, total energy, and charge density for the isolated molecules are calculated using a cubic supercell (with a side of nearly 16 Å). These quantities allow us to compute surface adsorption energies as well as induced dipole moments (Sec. II C).

B. Electron affinity and ionization potential

The electron affinity (EA) at a semiconductor surface is the energy needed to carry an electron from the vacuum to the bottom of the conduction band (CBM). Similarly, the ionization potential (IP) is defined as the energy required to bring an electron from the maximum of the valence band (VBM) to the vacuum.[19–22] The EA is calculated at DFT level as the energy difference between the vacuum level (E_{vac}) and the Kohn-Sham (KS) eigenvalue relative to the bottom of the conduction band of the semiconductor bulk band structure: $\chi=E_{vac}-E_{CBM}$. In the same way, the IP is computed as $I=E_{vac}-E_{VBM}$, where E_{VBM} corresponds to the top of the bulk valence band. While E_{VBM} and E_{CBM} are obtained from bulk band structure calculations, E_{vac} can be derived from a slab calculation, so that the energy references for these two systems could be, in general, different. This problem is nicely solved, thanks to the alignment procedure described in Sec. II A.

C. Vacuum level and surface dipole

The presence of adsorbates on a surface may induce, as already mentioned, changes in the vacuum level.[23,24] Here, we summarize the main concepts related to it. By symmetry, only the dipole component along the surface normal (assumed to be the z direction in the following) is responsible for the vacuum level modification. For the sake of simplicity, in the following, planar averages will be labeled with the same symbol as the corresponding functions.

Let $\rho(x,y,z)=\rho_{el}(x,y,z)+\rho_{ion}(x,y,z)$ be the total charge density of a given slab (ρ_{el} and ρ_{ion} give the electronic and ionic contributions to it, respectively). Its planar average can be defined as follows:

$$\rho(z)=\frac{1}{A}\int\int_{A} dxdy\ \rho(x,y,z), \tag{1}$$

where the integral is done on the surface unit cell and A is its area. An analogous definition can be given for the planar average $V(z)$ of the electrostatic potential $V(x,y,z)$.

The z component of the dipole moment per unit surface (in the following referred to as dipole moment density) can be related to the electrostatic potential using Eq. (1) and the Poisson's equation

$$p = \int_0^{c/2} dz\, z\rho(z) = -\frac{1}{4\pi} \cdot \int_0^{c/2} dz z \frac{1}{A} \times \left[\int \int_A dxdy \left(\frac{\partial^2 V}{\partial x^2} + \frac{\partial^2 V}{\partial y^2} + \frac{\partial^2 V}{\partial z^2} \right) \right]. \quad (2)$$

The integration extremes are $z=0$ (center of the slab) and $z=c/2$ (at the middle of the vacuum region). On the right side, the terms containing the partial derivative of V with respect to x and y give a zero contribution to the integral. The remaining term can be integrated by part, giving

$$p = \frac{1}{4\pi} \left[V\left(\frac{c}{2}\right) - V(0) \right]. \quad (3)$$

The vacuum level can be expressed as $E_{vac}=-eV(c/2)=-eV_{vac}$.

It will be useful to label with different superscripts the quantities p and V for clean (p^{cl}, V^{cl}) and covered (p^{co}, V^{co}) surfaces, respectively. By means of the alignment procedure previously depicted (see Sec. II A), at the center of the slab, V^{co} and V^{cl} overlap reproducing the bulk oscillating potential, so that at the center of the slab, we have $V^{co}(0)=V^{cl}(0)$. This is an important point because it shows that a variation of the surface dipole density $\Delta p=p^{co}-p^{cl}$ induced by the coverage induces, in turn, a proportional variation of the vacuum level energy $\Delta E=-e(V^{co}_{vac}-V^{cl}_{vac})$. Taking into account Eq. (3), it follows that

$$\Delta E = -4\pi e \Delta p. \quad (4)$$

The EA and IP change by the same amount, since their variations are only due to the vacuum level changes. From now on, we will focus on EA and IP changes with respect to the clean surface. The EA and IP values, for each system, can be obtained by adding the corresponding variation ΔE to the EA and IP of the clean surface, respectively. If we express the energy in rydbergs and the dipole density in a.u.$^{-1}$ [namely, define $\tilde{\chi}=\chi/(e^2/2a_B)$, $\tilde{p}=pa_B/e$, with a_B the Bohr radius], Eq. (4) becomes (for the EA, the same applies to the IP)

$$\Delta\tilde{\chi} = -8\pi\Delta\tilde{p}. \quad (5)$$

Finally, it is worthwhile stressing that, with the conventions used here, a positive dipole is oriented outward and causes a negative shift of the EA.

III. RESULTS AND DISCUSSIONS

A. Isolated molecules

We consider ethylene and a class of cyclopentene derivatives C_5H_6-R_1R_2 shown in Fig. 1. For cyclopentene [Fig. 1(a)] $R_1=R_2=$H, while one of these two H atoms is replaced with a functional group in the other cases. It turns out that two nonequivalent configurations are obtained if a given functional group replaces either R_1 or R_2. They will be referred to as the "axial" and "equatorial" configurations: for example, Figs. 1(b) and 1(c) show a substitutional amino (NH_2) group in axial and equatorial configurations, respectively. A bond to the ring atoms is termed axial or equatorial according to whether it makes a relatively large or small angle, respectively, with the plane containing or passing closest to a majority of the ring atoms. The five molecules shown in Fig. 1 correspond to (a) cyclopentene (C_5H_8), (b) axial-4-amino-cyclopentene ($C_5H_6NH_2H$), (c) equatorial-4-amino-cyclopentene ($C_5H_6HNH_2$), (d) axial-4-(2,5-dicyano-toluene)-cyclopentene ($C_5H_6C_9N_2H_5H$), and (e) equatorial-4-cyano-cyclopentene (C_5H_6HCN). The total dipole moments computed for this set of molecules are reported in Table I. Black arrows in Fig. 1 indicate the orientation of these dipole moments.

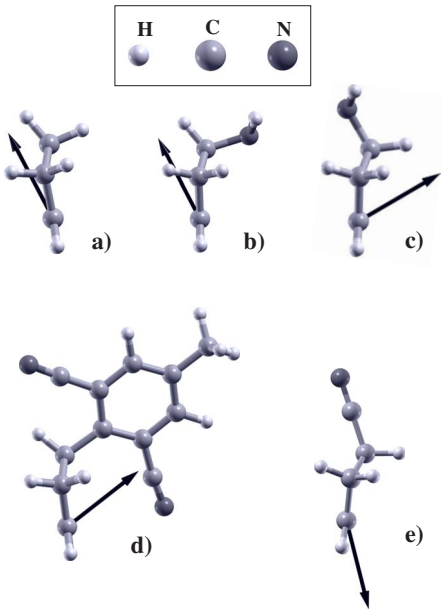

FIG. 1. (Color online) A ball-and-stick plot of the cyclic molecules C_5H_6-R_1R_2 investigated in this work, with (a) $R_1=R_2=$H (cyclopentene), (b) $R_1=$H, $R_2=NH_2$, (c) $R_1=NH_2$, $R_2=$H, (d) $R_1=C_9N_2H_5$, $R_2=$H, and (e) $R_1=$H, $R_2=$CN. Black arrows indicate the direction of the dipole moment of the isolated molecule.

B. Silicon surfaces

1. (001)-(2×2) *clean surface*

As mentioned before, the $p(2\times2)$ reconstruction of the clean Si(001) surface leads to the formation of dimer rows,

TABLE I. The computed dipole moment of the isolated molecules.

	$\|\mu\|$ (D)
C_2H_4	0.0
C_5H_8	0.270
$C_5H_6NH_2H$	1.368
$C_5H_6HNH_2$	1.242
$C_5H_6C_9N_2H_5H$	3.316
C_5H_6HCN	4.247

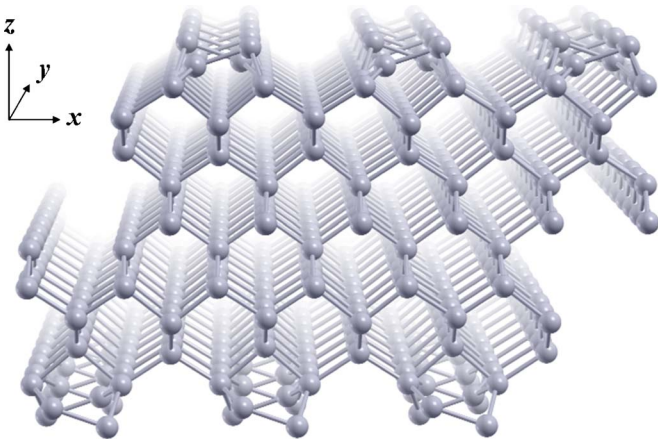

FIG. 2. (Color online) A perspective of the silicon (001) surface in the $p(2\times2)$ reconstruction. Dimers are alternately buckled along the dimer rows.

along which Si-Si dimers are alternately buckled (see Fig. 2). The calculated buckling angles[25] (about 19°) and dimer bond length (2.37 Å) are in a good agreement with the experimental results.[26]

An interesting point coming from our calculations is that the buckling of the atomic layers is not limited to the dimer (considered as the first layer) formation. The buckling can be quantified as the difference Δz between the z coordinates of two neighbor Si atoms along the dimer direction (such atoms belong to the same layer in the unreconstructed surface). As shown in the left panel of Fig. 3, the dimer buckling (Δz =0.76 Å) is clearly the most relevant, but also the third and the fourth layers show a significant buckling (Δz=0.27 Å and Δz=0.20 Å, respectively).

Concerning the electronic band structure, surface states lying in the bulk silicon band gap appear, associated with the dangling bonds originated by the $p(2\times2)$ surface reconstruction. As indicated in Fig. 4(a), these surface states can be distinguished in π bonding (π_1, π_2) and π^* antibonding (π_1^*, π_2^*) states. A qualitative agreement is found with other theoretical calculations of the silicon surface band structure.[25]

The EA and IP which we compute for the clean surface are χ=4.31 eV and I=4.96 eV, respectively (at the generalized gradient approximation level). It is also possible to evaluate a range of variability for the work function $\phi = E_{vac} - E_{FL}$ defined as the energy difference between the vacuum and the Fermi level (FL). At variance with metals, the work function (WF) of a semiconducting material is not an intrinsic property,[22] simply because the position of the Fermi energy in the forbidden energy gap depends on the experimental conditions (e.g., the doping). However, the presence of surface states in the band-gap region, as in the case of silicon, causes the well known pinning[27–29] of the Fermi level. Our computed WF range is 4.93–5.11 eV, in very good agreement with other theoretical works.[22] To match theoretical values to experimental results, one should use quasiparticle corrections (e.g., within the GW many-body approximation[30]) to the computed KS eigenvalues. In Ref. 22, a fair agreement with experimental results[31–34] for the WF is found using the GW corrected values.

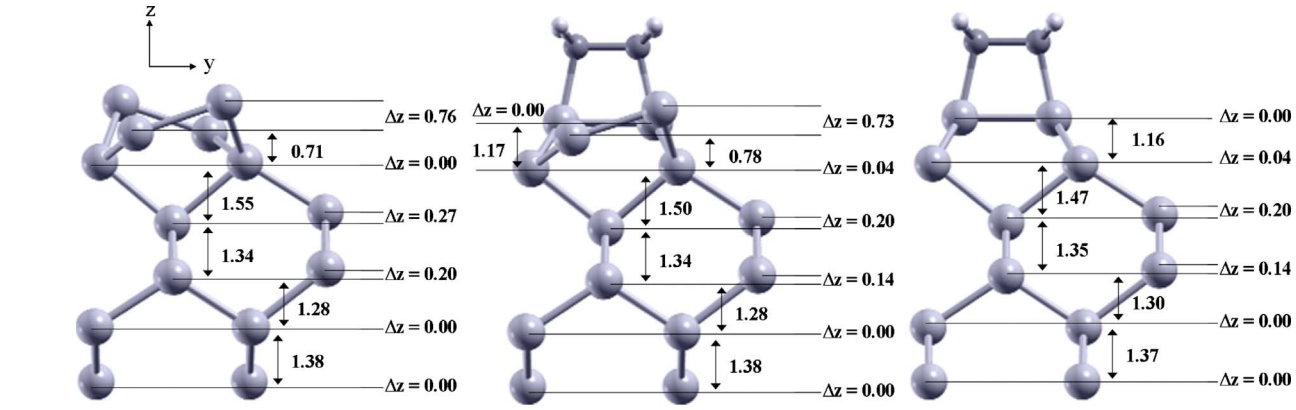

FIG. 4. (Color online) Surface band structure for the (a) clean surface and (b) half and (c) fully covered Si(001):C_2H_4 surfaces. Filled and empty states are indicated with solid and dashed lines, respectively. The shaded regions represent the projection of the bulk band structure in the two-dimensional surface Brillouin zone. The top of the bulk valence band is set at zero. The surface states π and π^* gradually disappear on increasing the coverage. The points J and J′ are defined in the same way as in Ref. 25.

FIG. 3. (Color online) Optimized geometries for the clean silicon (001) surface (left panel) and the half (central panel) and fully (right panel) covered Si(001):C_2H_4. Both the buckling Δz and the interlayer distances are given in Å.

2. (001)-(2×2):C_2H_4

The adsorption of ethylene on the Si(001) surface occurs through the [2+2] cycloaddition reaction. The relaxed geometries are computed for both half coverage, which is one molecule per dimer pair [or 0.5 ML (monolayer)], and full coverage, which is one molecule per dimer (or 1 ML). As already stated above, both the π component of the C═C bond and the π-like component of the Si dimer bond break leading to the formation of two C—Si σ bonds. As such, the cycloaddition leads to the unbuckling (Δz=0.00 Å) of the involved dimer (see Fig. 3, central and right panels) without changes on the dimer bond length (the σ component of the bond is preserved[35]). The C—C bond length after adsorption is 1.56 Å, in good agreement with the experimental result[26] of 1.62±0.08 Å. Moreover, the computed value is much closer to a C—C single bond than to a double one, as shown by the comparison between ethane (C_2H_6) and ethylene (C_2H_4). In the case of ethane, the C atoms are singly bonded with a bond length[36] of 1.535 Å and sp^3 hybridized with a ∢CCH measured angle[36] of 111.17° to be compared with the one (112.6°) we computed for the adsorbed ethylene. These results confirm the C—C double bond breaking and the sp^3 hybridization of the same C atoms as a consequence of the cycloaddition reaction.

The layer buckling difference between clean and covered surfaces is mainly restricted to the first layer, where the dimer involved in the cycloaddition is unbuckled. In fact, with a 0.5 ML coverage, only one dimer per pair is unbuckled (see Fig. 3, central panel), while both dimers in the surface unit cell are unbuckled with a 1 ML coverage. As clearly shown in Fig. 3 (central and right panels), also a variation with respect to the clean surface is found on the third and the fourth layers (buckling of Δz=0.20 Å and Δz =0.14 Å, respectively). A general trend toward the reduction of the buckling with the coverage is observed, and it is interesting to note that also the distance between the second and the third layers gradually decreases on increasing the coverage, going from 1.55 Å (clean surface) to 1.47 Å (1 ML coverage).

Focusing on the electronic properties, the surface states (clearly related to the Si-Si dimer) are gradually removed as the coverage increases and disappear at full coverage, as shown by comparing the near-gap band structures in Fig. 4 (the shaded areas are projections of the bulk band structure in the two-dimensional surface Brillouin zone). The ethylene adsorption induces EA changes of $\Delta\chi$=−0.64 eV for 0.5 ML and $\Delta\chi$=−1.17 eV for 1 ML coverage.

An interesting comparison with recent experimental data[37] can be done in the case of full coverage. In Ref. 37, a detailed study is reported on the adsorption of C_2H_4 on an *n* doped Si (001) surface. From their data, we can extract a value of the work function of 3.2 eV to be compared with our calculated value of 3.14 eV. Although the agreement is very good, it is necessary to detail the assumptions we have used for obtaining 3.14 eV. The first point is that at full coverage, there are no surface states in the band gap, as shown in Fig. 4(c). This means that at room temperature, the Fermi level is, because of doping, just below the bottom of the conduction band. It is therefore reasonable to assume that in this particular case, there is a negligible contribution from band bending so that work function and electron affinity are nearly the same. Our 3.14 eV is the difference between the vacuum level and the conduction band bottom.

There is another interesting observation to be made. The paper of Livneh and Asscher[38] discusses the results of measurements concerning work function variations during C_2H_4 adsorption on the Ru (001) surface. The point is that these authors have shown that the nature of C_2H_4 bonding on this metal is similar to the one discussed in this work, being the bonding due to an sp^3 hybridization. At full coverage, they measure a work function variation of −1.31 eV. Now, if we take our full coverage $\Delta\chi$=−1.17 eV, we see that there is some consistency between these values. If we consider that the ratio between the Si(001) surface unit cell area and that of the Ru (001) surface is roughly 1.19, our $\Delta\chi$ must be multiplied by 1.19 giving −1.39 eV, which is very near to the experimental estimate of −1.31 eV. It appears from this simple estimate that provided that the type of bonding on a surface does not change dramatically upon changing the material,[39] the electron affinity variations are, somehow, transferable properties. However, a more clear assessment of this interesting point would require specific calculations which, at the moment, are beyond the aim of this work.

TABLE II. The Si—C bond length for the different adsorbates and coverages.

	Half coverage	Full coverage
C_2H_4	1.955	1.959
C_5H_8	1.960	1.976
$C_5H_6NH_2H$	1.957	1.973
$C_5H_6HNH_2$	1.962	1.970
$C_5H_6C_9N_2H_5H$	1.966	
C_5H_6HCN	1.964	1.970

3. (001)-(2×2):C_5H_6-R_1R_2

A question arises on whether the bonding properties (bond lengths and angles) are the same or not for different molecular adsorbates, all anchoring to the surface through the same mechanism. In Table II, we report the computed Si—C bond length for the different adsorbates and both at half and full coverages. It is seen that a significant dependence on the adsorbate species is not found. Only a small increase of the bond length with coverage can, in fact, be observed. Similarly, dimer buckling and interlayer distance do not show appreciable differences with respect to the ethylene case (see Fig. 3).

Concerning the electronic properties, in a previous work, we have already shown that no signature in the midgap region can be detected[40] due to the adsorption of this class of molecules (the results are very similar to those shown in Fig. 4 in the case of ethylene). Only low-lying electronic bands depend on the adsorbate, in agreement with some experimental results.[41]

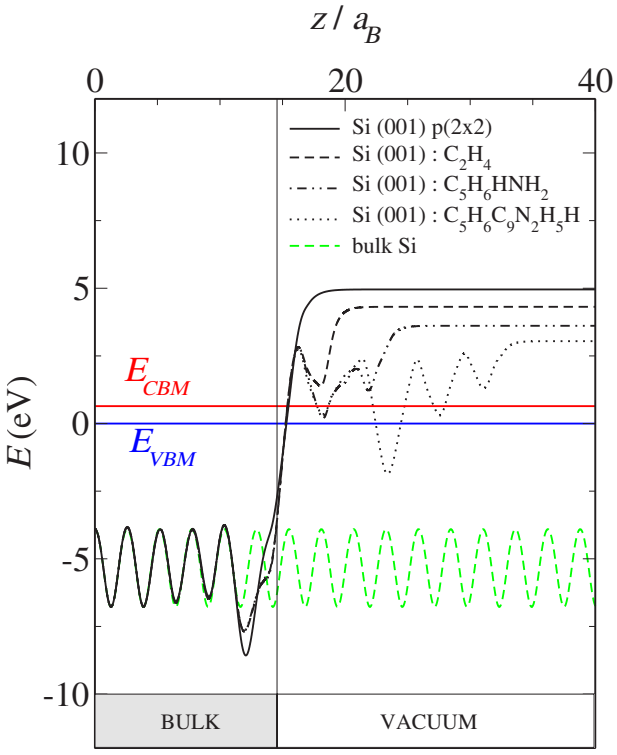

FIG. 5. (Color online) The planar average of the electrostatic potential for bulk Si and clean and (half) covered silicon (001) surfaces. Bulklike oscillations, independent of the adsorbed molecule, are obtained in the middle of the slab. E_{VBM} and E_{CBM} represent the top of the bulk valence band and the bottom of the bulk conduction band, respectively.

In Fig. 5, we show the averaged electrostatic energy for a 0.5 ML coverage of the different surface-adsorbate complexes. Bulklike oscillations (independent of the adsorbate species) can be observed in the middle of the slab (z=0) in all the cases. More interestingly, the shift in the vacuum level position with respect to the clean surface is clearly visible. From this shift, we compute $\Delta\chi$ for all the adsorbates and coverages, as summarized in the first column of Table III.

From both Fig. 5 and the corresponding values listed in Table III, it emerges very clearly the possibility of tuning the organic-semiconductor interface as far as the transfer of electrons is concerned.

Cycloaddition involving cyclic alkenes causes a complex structural deformation. In order to study these effects in a systematic way, we introduce the buckling angles φ_1, φ_2, and φ_3 as shown in Fig. 6. The C—C and Si—Si bonds involved in the cycloaddition nearly lie in the same plane (except for $C_5H_6C_9N_2H_5H$) so that the two Si—C bonds per molecule show nearly the same buckling angle φ_1, suggesting the use of the average value as a deformation parameter. For the same reason, the φ_2 and φ_3 averages are considered. The molecule reconstruction due to the adsorption can be viewed as a two-step effect, that is, the orientation of the molecule with respect to the surface and the deformation of the cyclic alkene structure. The former is related to φ_2, and the latter to φ_3.

In Fig. 7, front (upper panels) and side (lower panels) views of the C_5H_6HCN molecule are shown in the (a) isolated and (b) adsorbed (0.5 ML) configurations. A simple scheme of the cyclic alkene structure is also represented in Fig. 7(c) for clarity. For a more direct comparison, the isolated molecules have been oriented so as to have the C_c—C_c bond [see Fig. 7(c)] oriented along the $[1\bar{1}0]$ direction and the same φ_2 as the adsorbed molecule. Different values of φ_3 for the isolated (φ_3^{iso}) and the adsorbed (φ_3^{ads}) configuration clearly show the deformation of the cyclic alkene structure after adsorption.

In the case of 0.5 ML, because the mutual distances between neighbor molecules are large (exception made for $C_5H_6C_9N_2H_5H$), all the molecules undergo approximately

TABLE III. Calculated EA variation $\Delta\chi$ (eV) and total surface dipole moment density variation Δp (in units of 10^{-3} e/a_B) with respect to the clean surface. The various contributions to Δp are reported [see Eq. (8)]. The last column is the adsorption energy (in eV), defined as in Eq. (10). Different adsorbates and both half and full coverages are considered.

	$\Delta\chi$	Δp	p_a	Δp_b	Δp_s	E_{ads}
			Half coverage			
C_2H_4	−0.642	1.878	2.113	−0.249	0.014	−1.794
C_5H_8	−0.834	2.440	2.488	−0.049	0.001	−1.534
$C_5H_6NH_2H$	−1.204	3.523	3.620	−0.104	0.008	−1.546
$C_5H_6HNH_2$	−1.344	3.930	3.941	−0.021	0.010	−1.501
C_5H_6HCN	0.114	−0.331	−0.214	−0.124	0.006	−1.534
$C_5H_6C_9N_2H_5H$	−1.912	5.592	5.736	−0.143	0.001	−1.441
			Full coverage			
C_2H_4	−1.165	3.409	3.546	−0.573	0.436	−1.770
C_5H_8	−1.394	4.078	4.236	−0.593	0.435	−0.935
$C_5H_6NH_2H$	−1.706	4.991	5.150	−0.593	0.435	−0.957
$C_5H_6HNH_2$	−1.828	5.346	5.673	−0.761	0.434	−1.039
C_5H_6HCN	1.826	−5.344	−4.634	−1.149	0.440	−0.853

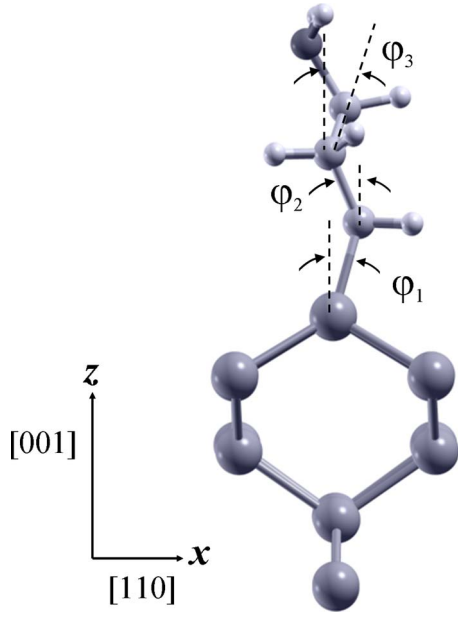

FIG. 6. (Color online) Buckling angles φ_1, φ_2, and φ_3, defined as angles between the projection of the corresponding bond onto the $(1\bar{1}0)$ plane (the xz plane in our case) and the [001] direction (the z axis).

the same deformation, as shown in Table IV. It means that the deformation of the cyclic structure is mainly related to the nature of the adsorption reaction (cycloaddition), whereas only a marginal role is played by both the functional group species and its position (equatorial or axial). As shown by a comparison between Figs. 7(a) and 7(b), the sp^3 hybridization of the C_c atoms leads to a new orientation of the C_c—H bonds. The C_c=C_c double bond breaking causes a significant variation of the C_c—C_c bond length and, as a consequence, a not negligible modification of the cyclic alkene structure. In fact, the variations of the H atom mutual distances are due to the rotation of the sp^3 structure of C_b

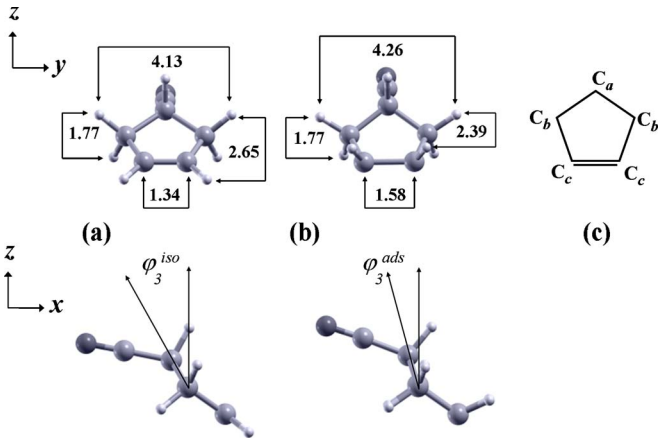

FIG. 7. (Color online) Front (upper panels) and side (lower panels) views of C_5H_6HCN in the (a) isolated and (b) adsorbed (0.5 ML) configurations. (c) A simple scheme of the cyclic structure is also shown for clarity. Some relevant distances are also reported (in Å).

TABLE IV. Buckling angles (in degrees, see Fig. 6 for their definition) for different adsorbed species and both 0.5 and 1 ML coverages.

	φ_1	φ_2	φ_3^{ads}	φ_3^{iso}
	Half coverage			
C_5H_8	−2	52	13	31
$C_5H_6NH_2H$	−4	50	10	33
$C_5H_6HNH_2$	−2	54	16	33
C_5H_6HCN	−1	55	18	31
	Full coverage			
C_5H_8	−14	27	27	6
$C_5H_6NH_2H$	−13	28	28	2
$C_5H_6HNH_2$	−15	23	−19	11
C_5H_6HCN	−14	24	−15	0

valence orbitals with respect to the isolated configuration. The reorientation of the C_b—C_a bonds corresponds to a rigid rotation of the C_a-R_1R_2 structure, as shown by comparing Figs. 7(a) and 7(b) for C_5H_6HCN.

In the case of 1 ML coverage, the mutual repulsion between neighbor molecules results on functional groups pointing outward with respect to the surface. For example, in the case of the amino-cyclopentene shown in Fig. 8, the equatorial and axial configurations show different values of φ_3^{ads} (see also Table IV), but the functional group is found at the same distance from the surface. This means that, on increasing the coverage, the cyclic alkene deformation becomes strongly dependent on the position of the functional group (equatorial or axial). We can conclude this analysis by observing that the structural change due to cycloaddition is not limited to the atoms directly involved in the reaction. In this sense, we can speak of nonlocal structural effects upon the molecule due to the cycloaddition reaction. Concerning the buckling of the silicon layers, no significant variation is obtained (at a fixed coverage) for all the adsorbates with respect to the case of C_2H_4, so that the surface deformation due to

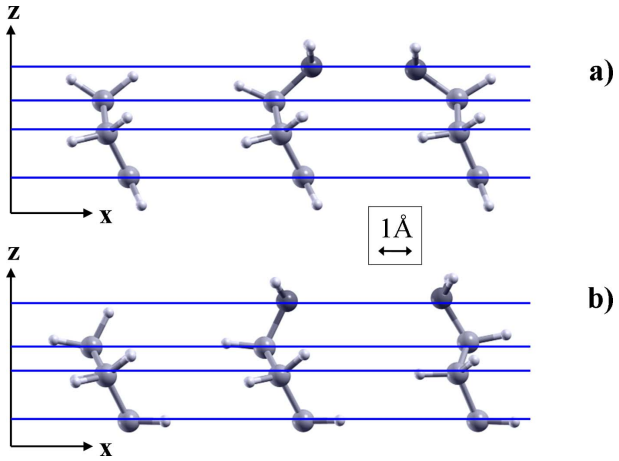

FIG. 8. (Color online) Side view of C_5H_8 (left panels), $C_5H_6HNH_2$ (central panels), and $C_5H_6NH_2H$ (right panels) in the (a) isolated and (b) adsorbed configurations at 1 ML coverage.

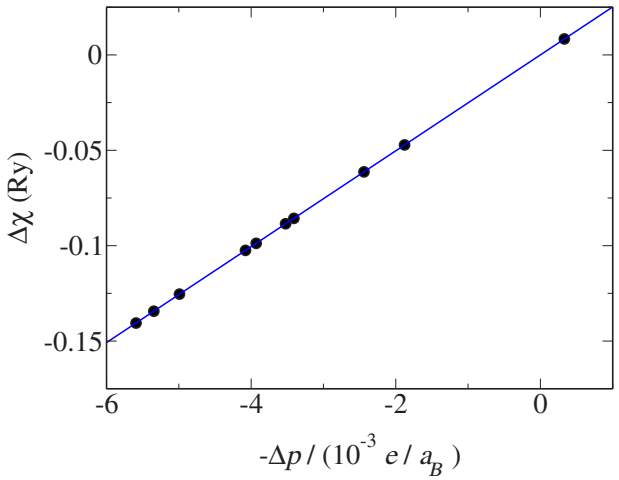

FIG. 9. (Color online) EA variation as a function of the surface dipole change due to the adsorption of the different molecules. Both coverages are represented.

adsorption is only connected to the nature of the reaction (the cycloaddition leads to the unbuckling of the Si—Si dimer) and the coverage.

C. Surface dipole analysis

In Sec. II C, we have shown that the functionalization of the surface produces an EA variation directly proportional to the surface dipole moment density variation Δp. The numerical values of $\Delta\tilde{p}$ [as calculated from Eq. (2)] and $\Delta\tilde{\chi}$ [as calculated as variation of the vacuum level, see Fig. 5] for all the cases studied fall closely on a solid line with a slope of 8π as expected from Eq. (5) and as shown in Fig. 9.

A closer inspection to the dipole layer induced by the adsorbate can be achieved if the different contributions to Δp are separated. The chemisorption process induces two main effects: a structural deformation of both the surface and the adsorbing molecule as discussed above and a charge transfer following the formation of the chemical bond. The two processes cannot be abstracted in reality, but a hypothetical two-step experiment can be simulated in the calculation. For a given surface-adsorbate system, we first compute the equilibrium relaxed geometry. Next, all the Si atoms are removed from the supercell and the total (ionic+electronic) charge density ρ_a of the isolated adsorbate layer is self-consistently computed. Finally, the adsorbate layer is removed from the supercell and the charge density ρ_s' of the silicon surface is computed. This allows us to get rid of charge density variations induced by relaxation, thus abstracting only the contribution coming from the formation of the chemical bonds.[24,42] In fact, the difference defined as $\Delta\rho_b=\rho-(\rho_a+\rho_s')$ is nothing else than the electron density redistribution due to the surface-molecule bond formation. The corresponding induced dipole density is

$$\Delta p_b = \int_0^{c/2} dz\, z\Delta\rho_b(z). \tag{6}$$

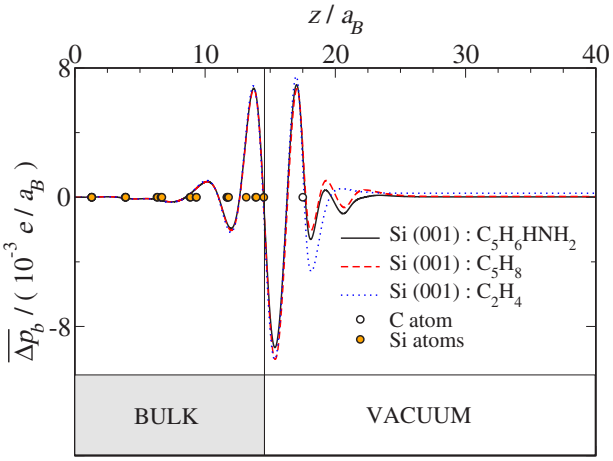

FIG. 10. (Color online) Cumulative sum of Δp_b [see Eq. (9)] at 0.5 ML coverage for C_2H_4, C_5H_8, and $C_5H_6HNH_2$.

By indicating with ρ_s the charge density of the clean surface, the total surface dipole variation (with respect to the clean surface) can be rewritten as follows:

$$\begin{aligned}\Delta p &= \int_0^{c/2} dz\, z(\rho-\rho_s)\\ &= \int_0^{c/2} dz\, z(\rho-\rho_a-\rho_s')\\ &\quad + \int_0^{c/2} dz\, z(\rho_s'-\rho_s) + \int_0^{c/2} dz\, z\rho_a\\ &= \Delta p_b + \Delta p_s + p_a,\end{aligned} \tag{7}$$

so that Eq. (5) becomes

$$\Delta\tilde{\chi} = -8\pi(\Delta\tilde{p}_b + \Delta\tilde{p}_s + \tilde{p}_a). \tag{8}$$

With this procedure, the total surface dipole moment density variation Δp can be viewed as made from the sum of three different contributions: $\Delta p_s=p_s'-p_s$, which is the variation of the surface dipole moment density due to the surface structural relaxation, Δp_b, the induced dipole moment density due to the formation of the chemical bond, and p_a, the projection on the z axis of the dipole moment of the molecule in the adsorbed configuration, divided by the surface unit cell area. The computed values are reported in Table III for half and full coverages. The data listed in this table may be complemented with the cumulative sum of Δp_b defined as

$$\overline{\Delta p_b}(z) = \int_0^z dz' z' \Delta\rho_b(z') \tag{9}$$

and shown in Fig. 10 for different adsorbates at 0.5 ML coverage. It is evident that $\overline{\Delta p_b}(c/2)=\Delta p_b$.

Figure 10 nicely shows that the variations of the dipole density associated with the formation of the chemical bond at and around the Si—C bonding sites are very similar for all the molecules considered. This is consistent with the very small differences in the Si—C bond length for different adsorbates shown in Table II. From Table III, it can be seen that

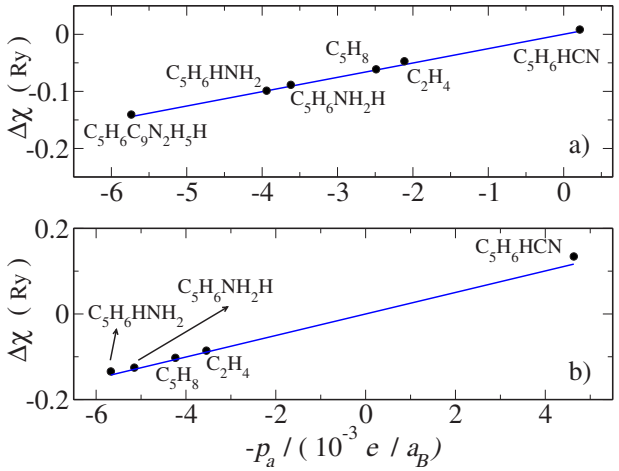

FIG. 11. (Color online) EA variation as a function of the projection of the dipole moment along the z axis (divided by the surface area) of the molecules in the adsorbed configuration (a) at 0.5 ML and (b) at 1ML coverages (see text).

the contribution of Δp_s is negligible at 0.5 ML, while it becomes comparable and opposite to Δp_b at 1 ML coverage. In any case, the main contribution to the total surface dipole variation Δp is represented by p_a.

In the last column of Table III, we report the adsorption energies for the different molecules at both half and full coverages. Such energy is defined as

$$E_{ads} = [E - (E_S + 2nE_m)]/2n, \tag{10}$$

where E is the total energy of the surface-molecule complex, E_S is the total energy of the $p(2\times2)$ reconstructed Si(001) surface, and E_m is total energy of the isolated molecule. Both E and E_S are referred to a 2×2 surface unit cell containing n molecules (1 or 2 for half and full coverages, respectively), and the factor of 2 takes into account the fact that molecules are adsorbed on both sides of the slab. It turns out that, at a fixed coverage, the mutual repulsion of neighbor molecules results in less stable structures for the surface-adsorbate complexes with the larger molecules. For the same reason, full coverage results in higher adsorption energies, with negligible difference only in the case of ethylene. No apparent correlation is found between adsorption energies and molecule dipole moments.

D. Can we correlate electron affinity variation to isolated molecule dipole moment?

In the previous section, we have seen that the main contribution to the surface dipole comes from p_a, defined as the z component of the dipole moment density of a molecular "layer" obtained by removing all the Si atoms from the supercell. In Fig. 11, we show the variations of electron affinity $\Delta\chi$ as a function of $-p_a$ for both (a) half coverage and (b) full coverage. Both the data point calculated from the electrostatic potential analysis (see Sec. II B and Table III) and the theoretical straight line [calculated from Eq. (5)] are reported. The main finding is that Eq. (5) is able to fit the calculated $\Delta\chi$ even if, at variance with Fig. 9, the p_a component of the dipole moment density is used, rather than its total variation Δp. This confirms that the main contribution to $\Delta\chi$ comes from p_a.

TABLE V. Dipole moment per molecule of the molecular slab (P_a/n, with $n=1$ or $n=2$ for 0.5 and 1 ML coverages, respectively) and of the isolated molecule (P_a^{is}) calculated with the geometry of the molecular adsorbate. The difference between the second and the first column is the depolarization contribution ΔP_a^{depol} (see text). The dipole moments are in units of ea_B.

	P_a/n	P_a^{is}	$-\Delta P_a^{depol}/P_a^{is}$
	Half coverage		
C_2H_4	0.452	0.492	0.08
C_5H_8	0.533	0.633	0.16
$C_5H_6NH_2H$	0.775	0.932	0.17
$C_5H_6HNH_2$	0.844	1.020	0.17
C_5H_6HCN	–0.046	–0.070	0.34
$C_5H_6C_9N_2H_5H$	1.228	1.819	0.32
	Full coverage		
C_2H_4	0.380	0.499	0.24
C_5H_8	0.453	0.649	0.30
$C_5H_6NH_2H$	0.551	0.731	0.25
$C_5H_6HNH_2$	0.607	0.793	0.23
C_5H_6HCN	–0.496	–0.853	0.42

In designing a particular interface, it may be important to know in advance whether or not we can estimate the EA variations from the knowledge of the properties of the isolated molecule (dipole moment, in this case).

We can calculate P_{is}, the z component of the dipole moment of the isolated molecule, after rotating each molecule, so as to have the same φ_2 buckling angle of the adsorbate, as previously depicted [see, for example, Figs. 7(a) and 8(a)]. In Fig. 12, we plot P_{is} versus $P_a = Ap_a$, where P_a is calculated at 0.5 ML coverage (both P_{is} and P_a are dipole moments rather than dipole moment densities). The straight line is a linear regression of the plotted points. It is seen that an evident correlation between the two dipole moments cannot be found. Combined with the results of Figs. 9 and 11, this shows that the nice agreement with Eq. (5) is lost if one

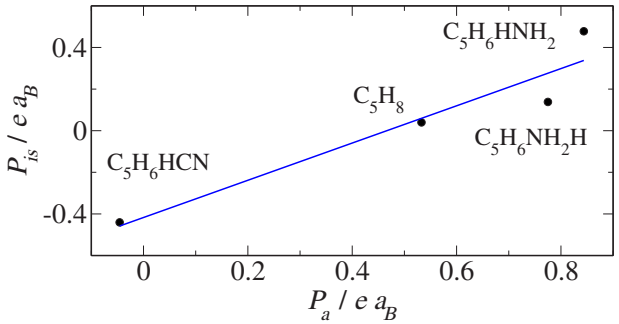

FIG. 12. (Color online) The projection of the dipole moment along the z axis for adsorbed (P_a) and isolated (P_{is}) configurations. It should be noted that in this figure, P_a and P_{is} are the dipole moments rather than the dipole moment densities.

constructs a plot using the dipole moment (or its z component) of the isolated molecule. This supports our picture of "nonlinear" effects induced by the surface-molecule bonding, associated with a significant geometrical deformation of the molecules.

Indeed, the adsorption induces a change in the hybridization of the two C_c atoms (see Fig. 7) from sp^2 to sp^3. The sp^3 orbitals show similar orientations for all the studied molecules (ethylene and cyclopentene derivatives), but this does not result in similar variations of the molecule dipole moment. As shown in Fig. 1, the dipole orientation strongly depends on the functional group and its position with respect to the molecule (equatorial or axial). As a result, similar changes and reorientations of the C_c sp^3 orbitals can cause different reorientation of the functional group and, in principle, different dipole moment variations.

We conclude by observing that "nonlinearity" in dipole moment variations could also be associated with depolarization effects. Simply because these are polarizable molecules, the dipole moment of the molecular layer P_a can be different from that of the isolated molecule even in the absence of any geometrical reorganization.[9] To get rid of such effects, we can related P_a with P_{is} through

$$P_a/n = (P_a/n - P_a^{is}) + (P_a^{is} - P_{is}) + P_{is} = \Delta P_a^{depol} + \Delta P_a^{relax} + P_{is}, \tag{11}$$

where the subscript a is always referred to the geometry of the adsorbed molecule. Here, P_a^{is} is the dipole moment of an isolated molecule (so no depolarization effects are included) having this geometry, whereas $\Delta P_a^{depol} = P_a - P_a^{is}$ and $\Delta P_a^{relax} = P_a^{is} - P_{is}$. Therefore, depolarization (ΔP_a^{depol}) and relaxation (ΔP_a^{relax}) effects have been separated out. If ΔP_a^{depol} is not zero, the coverage induces molecule-molecule interactions that modify its dipole moment even if no relaxation effects would take place. In Table V, we show the dipole moment variations associated with depolarization effects. It turns out that depolarization effects may determine changes in the isolated molecule dipole moment from 8% to about 40%. Such changes are larger for full coverage. Nonetheless, a plot of ΔP_a^{depol} versus P_a/n shows linear correlation between the two. Therefore, the previous conclusion that it is not possible to correlate the changes in the electron affinity with the dipole moment of the isolated molecule should be attributed to (nonlinear) effects induced by distortion, namely, ΔP_a^{relax}, rather than polarization effects.

IV. CONCLUSION

In this work, we have given a detailed description of the formation of a dipole layer due to the adsorption of ethylene and of a class of organic molecules with the general formula C_5H_6-R_1R_2, where R_1 and R_2 are functional groups controlling the molecular dipole moments. We have seen that although these molecules adsorb on the silicon (001) surface through the same mechanism, both the silicon substrate and the molecule geometry have a reconstruction which depends on both the molecule type and the coverage. These reconstructions induce a significant variation in the surface dipole moment, which results in a corresponding variation of the electron affinity. A detailed analysis of the various contributions to the surface dipole has revealed that the common practice of linking the electron affinity variations directly to the dipole moment of the isolated molecule is, as a rule, not always correct. The exception to this rule is when a molecule, after adsorption, does not change its geometry. A particularly interesting case is that of the benzoic acids with different parasubstituents that control the dipole moment. Measurements of the electron affinity do show a clear linear relation with the dipole of the isolated molecule and this is due to the fact that the bonding to the surface does not corrupt the benzene ring.[43–45] In other words, while the cycloaddition reaction with the molecules considered in this work gives rise to a reconstruction which changes the geometry and the orientation of the molecule, it is likely that this does not occur with the benzoic acids.

ACKNOWLEDGMENTS

We acknowledge the support of the MIUR PRIN (2005) Italy. The calculations were performed at CINECA-Bologna "Iniziativa Calcolo Parallelo del CNR-INFM."

*ivo.borriello@na.infn.it

[1] R. A. Wolkov, Annu. Rev. Phys. Chem. **50**, 413 (1999), and references therein.

[2] J. M. Buriak, Chem. Rev. (Washington, D.C.) **102**, 1271 (2002), and references therein.

[3] M. A. Filler and S. F. Bent, Prog. Surf. Sci. **73**, 1 (2003), and references therein.

[4] R. J. Hamers, S. K. Coulter, M. D. Ellison, J. S. Hovis, D. F. Padovitz, M. P. Schwartz, C. M. Greenlief, and J. N. Russel, Jr., Acc. Chem. Res. **33**, 617 (2003), and references therein.

[5] J. Yoshinobu, Prog. Surf. Sci. **77**, 37 (2004).

[6] D. Alexson, H. Chen, M. Cho, M. Dutta, Y. Li, P. Shi, A. Raichura, D. Ramadurai, S. Parikh, M. A. Stroscio, and M. Vasudev, J. Phys.: Condens. Matter **17**, R637 (2005), and references therein.

[7] H. Fukagawa, S. Kera, T. Kataoka, S. Hosoumi, Y. Watanabe, K. Kudo, and N. Ueno, Adv. Mater. (Weinheim, Ger.) **19**, 665 (2007).

[8] G. Witte, S. Lukas, P. S. Bagus, and C. Wöll, Appl. Phys. Lett. **87**, 263502 (2005).

[9] V. De Renzi, R. Rousseau, D. Marchetto, R. Biagi, S. Scandolo, and U. del Pennino, Phys. Rev. Lett. **95**, 046804 (2005).

[10] B. Duke, Chem. Rev. (Washington, D.C.) **96**, 1237 (1996).

[11] S. Y. Quek, J. B. Neaton, M. S. Hybertsen, E. Kaxiras, and S. G. Louie, Phys. Rev. Lett. **98**, 066807 (2007).

[12] G. Festa, M. Cossi, V. Barone, G. Cantele, D. Ninno, and G. Iadonisi, J. Chem. Phys. **122**, 184714 (2005).

[13] S. Baroni, A. Dal Corso, S. de Gironcoli, P. Giannozzi, C. Cavazzoni, G. Ballabio, S. Scandolo, G. Chiarotti, P. Focher, A. Pasquarello, K. Laasonen, A. Trave, R. Car, N. Marzari, and A. Kokalj, http://www.quantum-espresso.org
[14] A. M. Rappe, K. M. Rabe, E. Kaxiras, and J. D. Joannopoulos, Phys. Rev. B **41**, R1227 (1990).
[15] J. P. Perdew, K. Burke, and M. Ernzerhof, Phys. Rev. Lett. **77**, 3865 (1996).
[16] *Numerical Data and Functional Relationship in Science and Technology*, edited by O. Madelung, Landolt-Börnstein, New Series, Group III, Vol. 17, Pt. A (Springer-Verlag, Berlin, 1982).
[17] H. J. Monkhorst and J. D. Pack, Phys. Rev. B **13**, 5188 (1976).
[18] E. Kaxiras, Y. Bar-Yam, J. D. Joannopoulos, and K. C. Pandey, Phys. Rev. B **33**, 4406 (1986).
[19] A. Many, Y. Goldstein, and N. B. Grover, *Semiconductor Surfaces* (North-Holland, Amsterdam, 1965).
[20] S. J. Sque, R. Jones, and P. R. Briddon, Phys. Rev. B **73**, 085313 (2006).
[21] D. Cahen and A. Kahn, Adv. Mater. (Weinheim, Ger.) **15**, 271 (2003).
[22] C. Sgiarovello, N. Binggeli, and A. Baldereschi, Phys. Rev. B **64**, 195305 (2001).
[23] M. J. Rutter and J. Robertson, Phys. Rev. B **57**, 9241 (1998).
[24] T. C. Leung, C. L. Kao, W. S. Su, Y. J. Feng, and C. T. Chan, Phys. Rev. B **68**, 195408 (2003).
[25] A. Ramstad, G. Brocks, and P. J. Kelly, Phys. Rev. B **51**, 14504 (1995).
[26] M. P. Casaletto, R. Zanoni, M. Carbone, M. N. Piancastelli, L. Aballe, K. Weiss, and K. Horn, Phys. Rev. B **62**, 17128 (2000).
[27] H. Lüth, *Surfaces and Interfaces of Solid Materials* (Springer, Berlin, 1995).
[28] J. Bardeen, Phys. Rev. **71**, 717 (1947).
[29] F. J. Allen and G. W. Gobeli, Phys. Rev. **127**, 150 (1962).
[30] G. Onida, L. Reining, and A. Rubio, Rev. Mod. Phys. **74**, 601 (2002).
[31] J. Günster, Th. Mayer, and V. Kempter, Surf. Sci. **359**, 155 (1996).
[32] Q. B. Lu, R. Souda, D. J. O'Connor, and B. V. King, Phys. Rev. B **54**, R17347 (1996).
[33] S. Kono, Y. Enta, T. Abukawa, and T. Kinoshita, Appl. Surf. Sci. **41-42**, 75 (1989).
[34] F. G. Allen, J. Phys. Chem. Solids **8**, 119 (1959).
[35] A. J. Fisher, P. E. Blöchl, and G. A. D. Briggs, Surf. Sci. **374**, 298 (1997).
[36] *Handbook of Chemistry and Physics*, 73rd ed. (CRC, Boca Raton, FL, 1992).
[37] F. Matsui, H. W. Yeom, I. Matsuda, and T. Ohta, Phys. Rev. B **62**, 5036 (2000).
[38] T. Livneh and M. Asscher, J. Phys. Chem. B **104**, 3355 (2000).
[39] M. M. Hills, J. E. Parmeter, C. B. Mullins, and W. H. Weinberg, J. Am. Chem. Soc. **108**, 3554 (1986).
[40] G. Cantele, F. Trani, D. Ninno, M. Cossi, and V. Barone, J. Phys.: Condens. Matter **18**, 2349 (2006).
[41] W. Widdra, A. Fink, S. Gokhale, P. Trischberger, D. Menzel, U. Birkenheuer, U. Gutdeutsch, and N. Rösch, Phys. Rev. Lett. **80**, 4269 (1998).
[42] M. Preuss, W. G. Schmidt, and F. Bechstedt, Phys. Rev. Lett. **94**, 236102 (2005).
[43] A. Vilan and D. Cahen, Trends Biotechnol. **20**, 22 (2002).
[44] J. Krüger, U. Bach, and M. Grätzel, Adv. Mater. (Weinheim, Ger.) **12**, 447 (2000).
[45] S. Bastide, R. Butruille, D. Cahen, A. Dutta, J. Libman, A. Shanzer, L. Sun, and A. Vilan, J. Phys. Chem. B **101**, 2678 (1997).